J Math Imaging Vis (2008) 32: 57–72
DOI 10.1007/s10851-008-0075-4

A Fourier Domain Framework for Variational Image Registration

Jorge Larrey-Ruiz · Rafael Verdú-Monedero · Juan Morales-Sánchez

Published online: 1 April 2008
© Springer Science+Business Media, LLC 2008

Abstract Image registration is a widely used task in image analysis, having applications in various fields. Its classical formulation is usually given in the spatial domain. In this paper, a novel theoretical framework defined in the frequency domain is proposed for approaching the multidimensional image registration problem. The variational minimization of the joint energy functional is performed entirely in the frequency domain, leading to a simple formulation and design, and offering important computational savings if the multidimensional FFT algorithm is used. Therefore the proposed framework provides more efficient implementations of the most common registration methods than already existing approaches, adding simplicity to the variational image registration formulation and allowing for an easy extension to higher dimensions by using the multidimensional Fourier transform of discrete multidimensional signals. The new formulation also provides an interesting framework to design tailor-made regularization models apart from the classical, spatial domain based schemes. Simulation examples validate the theoretical results.

Keywords Image registration · Variational methods · Fourier transforms · Multidimensional signal processing

This work is partially supported by the Spanish Ministerio de Educación y Ciencia, under grant TEC2006-13338/TCM, and by Fundación Séneca, project 03122/PI/05.

J. Larrey-Ruiz (✉) · R. Verdú-Monedero · J. Morales-Sánchez
Information Technologies and Communications, Technical University of Cartagena, 30202 Cartagena, Spain
e-mail: jorge.larrey@upct.es

1 Introduction

Image registration is the process of finding an optimal geometric transformation that aligns points in one view of an object with corresponding points in another view of the same object or a similar one. Particularly, in medical imaging there are several applications that require a registration step (e.g. image fusion, atlas matching, pathological diagnosis). For an overview on registration methods, we refer to e.g. [8, 46], and more precisely to [24, 32, 34], and references therein, for medical image registration.

The image registration problem is known to be an ill-posed one, since it does not satisfy Hadamard's criterion. Therefore it becomes necessary to impose a deformation model to the registration algorithm, otherwise the motion of a point would be estimated independently of the motion of neighboring points, thus yielding a very discontinuous and unlikely displacement field. The deformation model should constrain the estimated transformation as much as possible using some prior knowledge on the deformation field [43]. In the literature, we find three major deformation models: *parametric models*, which constrain the estimate of the transformation to belong to a low dimensional transformation space by solving the minimization of some type of geometrical distance between the images to be registered [22, 41]; *competitive models*, which rely on the use of a regularization energy that depends on the displacement field, therefore penalizing a transformation proportionally to its irregularity, measured by the regularization energy with eventual additional boundary constraints [35]; and *incremental models*, which also rely on the use of a regularization energy, although in this case it does not depend on the transformation itself, but on its evolution (e.g. viscoelastic approach presented in [10]). When classified according to the image features used to recover the transformation, registration al-

gorithms are usually parted into three groups: *geometric feature based*, which rely on the segmentation, done generally before the registration process itself, of part or all of the images, therefore obtaining objects that are registered by minimizing some geometrical distance between them; *intensity based*, which minimize a intensity similarity measure (typically the sum of squared differences, the mutual information or the correlation ratio) computed between points lying at the same spatial position; and *iconic feature based*, which are really intermediate between the two previous categories, since they use explicitly some type of geometrical distance in addition to the intensity similarity measure, see [9]. In this work, we will focus on the intensity based registration with competitive regularization model, which is one of the most widely used registration scenarios in the literature, since it is a highly reliable and flexible one (see e.g. [25, 44]). This problem can be approached by using a variational principle which leads to the Euler-Lagrange partial differential equations (PDEs) [18, 31]. The computation of a numerical solution for the resulting registration scheme in the spatial domain is not straightforward, and there is no a simple alternative formulation. Some attempts to come up with fast algorithms can be found e.g. in [6], where a convolution kernel in scale-space is used, [16], where an additive operator splitting scheme is proposed, [30], where the multiscale nature of the image registration is exploited, or [11], where steepest descent methods are combined with implicit and semi-implicit iterative schemes. The aim of this work is twofold: to provide a novel theoretical framework which allows for an efficient implementation of variational registration methods in the frequency domain; and to allow for an easy extension to higher dimensions by using the d-dimensional Fourier transform of discrete multidimensional signals. The variational equations are translated into the frequency domain by means of Parseval's theorem, thus obtaining the Euler-Lagrange equations defined in the frequency domain, which serve as a starting point for all implementations.

The paper is organized as follows: we start out with a review of the mathematical formulation of the general registration problem in the spatial domain. In the following section, the proposed framework for image registration, defined entirely in the frequency domain, is presented. Next, the implementation aspects of the resulting registration schemes, as well as an efficiency comparison, are tackled. In Sect. 5, the frequency domain based framework is tested on two medical imaging experiments. Finally, the conclusions close the paper.

2 Variational Formulation in the Spatial Domain

Let R and T be two data sets, a reference and a template respectively, which represent the same object (or similar ones) by using the same or different imaging modalities. We assume that the data sets can be represented by compactly supported functions $R,\ T : \Psi \subset \mathbb{R}^d \to \mathbb{R}$, where $\Psi :=]0, 1[^d$ and d denotes the number of spatial dimensions of the data sets. Usually, these data sets are two- or three-dimensional. This means, the map associates to each spatial position $\mathbf{x} = (x_1, \ldots, x_d)^\top \in \Psi$ the intensities $T(\mathbf{x})$ and $R(\mathbf{x})$, on a bounded domain with Lipschitz boundary $\partial\Psi$. We search for a displacement field $\mathbf{u} : \mathbb{R}^d \to \mathbb{R}^d$ that makes the transformed template data set similar to the reference data set in the geometrical sense, i.e., $T_{\mathbf{u}}(\mathbf{x}) := T\,(\mathbf{x} - \mathbf{u}(\mathbf{x})) \approx R(\mathbf{x})$, where $\mathbf{u}(\mathbf{x}) = (u_1(\mathbf{x}), \ldots, u_d(\mathbf{x}))^\top$. This problem can be approached in terms of the variational calculus [2, 45], by defining the joint energy functional to be minimized:

$$\mathcal{J}[\mathbf{u}] := \mathcal{D}[R, T; \mathbf{u}] + \alpha\, \mathcal{S}[\mathbf{u}], \tag{1}$$

where $\mathcal{D}$ is an energy term which measures the disparity between the transformed data set and the reference data set, $\mathcal{S}$ is a penalty term which measures the roughness of the displacement field and acts as a regularization term, penalizing unwanted deformations, and $\alpha > 0$ is a scalar parameter, usually referred to as the regularization parameter, which is used to control and weight the influence of the regularization term versus the distance term.

The choice of the distance measure $\mathcal{D}$ depends on the particular data sets to be registered. When the intensities of the data sets are similar (i.e., in a monomodal registration scenario), the sum of squared differences (SSD) or the sum of absolute differences (SAD) of the data sets are commonly used [8, 36]. When dealing with data sets from different sources or modalities (i.e., in a multimodal registration scenario), statistical measures such as the mutual information (MI) [13, 33] or the correlation ratio (CR) [31, 40] are the most appropriate choices.

The regularization term $\mathcal{S}$ is used to circumvent the ill-posedness of the non-rigid registration problem by adding some prior knowledge of the deformation, thus preferentially obtaining more likely solutions, and giving the smoothness characteristics to the displacement field. In the literature (see e.g. [23]), the most widely used regularization terms for image registration can be expressed as

$$\begin{aligned}\mathcal{S}[\mathbf{u}] &:= \frac{1}{2}\, a[\mathbf{u}, \mathbf{u}] = \frac{1}{2} \int_\Psi \big\langle \mathcal{B}[\mathbf{u}], \mathcal{B}[\mathbf{u}] \big\rangle_{\mathbb{R}^d}\, d\mathbf{x} \\ &= \frac{1}{2} \int_\Psi \big\langle \mathcal{A}[\mathbf{u}], \mathbf{u} \big\rangle_{\mathbb{R}^d}\, d\mathbf{x}, \end{aligned} \tag{2}$$

where $a[\mathbf{u}, \mathbf{u}] \in \mathbb{R}$ is a positive bilinear form, $\mathcal{B}$ and $\mathcal{A}$ are partial differential operators, and $\langle \cdot, \cdot \rangle_{\mathbb{R}^d}$ denotes the dot (or inner) product in $\mathbb{R}^d$. The particular definition of $\mathcal{S}$ results in different registration methods. The most popular are the following [20]:

1. *Elastic registration*, where the regularization is based on the linearized elastic potential of the displacement field, therefore penalizing the tension or *inner stress* in

the transformed template, which is considered a clamped elastic membrane [3, 7]. The expression for this regularizer is

$$\mathcal{S}^{\text{elas}}[\mathbf{u}] := \int_\Psi \frac{\mu}{4} \sum_{l,m=1}^{d} \left(\partial_{x_l} u_m + \partial_{x_m} u_l\right)^2 + \frac{\lambda}{2} (\operatorname{div} \mathbf{u})^2 \, d\mathbf{x}, \tag{3}$$

where $\lambda \geq 0$ and $\mu > 0$ are the Lamé constants which reflect material properties.[1]

2. *Fluid registration*, where the regularization is based on the elastic potential of the time derivative of the displacement, i.e., this method is characterized by the spatial smoothing of the velocity field of a fluid model. Then, in principle, any displacement can be obtained given enough time: the internal stresses disappear eventually [6, 12]. The penalty term for fluid registration is described by

$$\mathcal{S}^{\text{fluid}}[\mathbf{u}] := \mathcal{S}^{\text{elas}}[\mathbf{v}], \tag{4}$$

where

$$\mathbf{v}(\mathbf{x}, t) := \frac{d}{dt}\mathbf{u}(\mathbf{x}, t) = \partial_t \mathbf{u}(\mathbf{x}, t) + \nabla \mathbf{u}(\mathbf{x}, t)\, \mathbf{v}(\mathbf{x}, t) \tag{5}$$

is the so-called velocity field.

3. *Diffusion registration*, which is based on the minimization of the energy of first-order spatial derivatives of the displacement field, thus admitting constant displacements, but penalizing oscillating deformations [16, 42]. The equation of this regularizer is

$$\mathcal{S}^{\text{diff}}[\mathbf{u}] := \frac{1}{2} \sum_{l=1}^{d} \int_\Psi \left\langle \nabla u_l, \nabla u_l \right\rangle_{\mathbb{R}^d} d\mathbf{x} = \frac{1}{2} \sum_{l=1}^{d} \int_\Psi \|\nabla u_l\|^2 \, d\mathbf{x}. \tag{6}$$

4. *Curvature registration*, which is based on the minimization of an approximation to the energy of curvature of the displacement field [17, 30], i.e., it is based on second-order spatial derivatives and therefore the regularization term can be neutral with respect to affine linear transformations if appropriate boundary conditions are imposed to the space of possible displacements [27]. The curvature smoother is defined by

$$\mathcal{S}^{\text{curv}}[\mathbf{u}] := \frac{1}{2} \sum_{l=1}^{d} \int_\Psi \left\langle \nabla^2 u_l, \nabla^2 u_l \right\rangle_{\mathbb{R}^d} d\mathbf{x} = \frac{1}{2} \sum_{l=1}^{d} \int_\Psi (\Delta u_l)^2 \, d\mathbf{x}, \tag{7}$$

where $\Delta := \nabla^2 = \nabla^\top \nabla$ is the d-dimensional Laplace operator.

According to the calculus of variations, a displacement field $\mathbf{u}$ which minimizes (1) is necessarily a solution of the Euler-Lagrange equation

$$\mathbf{f}(\mathbf{x}; \mathbf{u}) + \alpha\, \mathcal{A}[\mathbf{u}](\mathbf{x}) = \mathbf{0} \tag{8}$$

subject to suitable boundary conditions [5], which are imposed in order to overcome the unsolved question of the existence of minima [30]. The so-called external forces field, $\mathbf{f}(\mathbf{x}; \mathbf{u})$, related to the distance measure $\mathcal{D}$, drives the deformation. On the other hand, the partial differential operator $\mathcal{A}$, related to the regularizer $\mathcal{S}$ (see (2)), can be seen as internal constraints which resist the external forces until the equilibrium state described by the set of partial differential equations (8) is achieved. For the registration methods considered in this work, the operator $\mathcal{A}$ is defined as (see [20])

$$\mathcal{A}^{\text{elas}}[\mathbf{u}](\mathbf{x}) = -\mu\, \Delta \mathbf{u}(\mathbf{x}) - (\lambda + \mu) \nabla \operatorname{div} \mathbf{u}(\mathbf{x}), \tag{9}$$

$$\mathcal{A}^{\text{fluid}}[\mathbf{u}](\mathbf{x}) = -\mu\, \Delta \mathbf{v}(\mathbf{x}) - (\lambda + \mu) \nabla \operatorname{div} \mathbf{v}(\mathbf{x}), \tag{10}$$

$$\mathcal{A}^{\text{diff}}[\mathbf{u}](\mathbf{x}) = -\Delta \mathbf{u}(\mathbf{x}), \tag{11}$$

$$\mathcal{A}^{\text{curv}}[\mathbf{u}](\mathbf{x}) = \Delta^2 \mathbf{u}(\mathbf{x}). \tag{12}$$

The resulting non-linear PDEs (8) can be solved numerically by using a finite difference approximation of $\mathcal{A}$ (Appendix shows the kernels of the discrete approximations used for the derivatives), and a fixed-point or time-marching semi-implicit iterative scheme [11]. The solution of (8) is commonly accomplished by reshaping the d-dimensional problem into a one-dimensional scenario (i.e., rearranging each d-dimensional matrix into a single column vector) [36, 45]. This provides an iterative procedure, characterized by a highly structured matrix which is large, sparse and often ill-conditioned, and that has to be inverted with special procedures [4, 15]. A popular strategy which does not require matrix inversions at all is to exploit the multiscale and/or multigrid nature of the registration problem, taking the spatially discretized scenario as a starting point [26, 30]. In particular, the numerical solution proposed for the latter approaches demands a preprocessing stage which includes a Cholesky factorization with high computational complexity (up to $\mathcal{O}(N^3)$) [28], and the results it produces are only

[1] As addressed in [36] or [29], the Lamé constants within the elastic and fluid registration scenarios are always chosen so that the changes allowed in the data sets are maximal and the lateral shrink is eliminated, i.e., by setting $\lambda = 0$ and $\mu > 0$.

approximations, not the exact ones [36]. Therefore the resulting scenario in the spatial domain implies considerable computational load and memory requirements.

3 Variational Formulation in the Frequency Domain

In order to overcome the previous drawbacks, this paper proposes a novel mathematical framework for the d-dimensional image registration scenario. The registration problem will be approached in terms of a variational formulation in the Fourier domain. As a result, we will be able to find a minimizer $\mathbf{u}$ for the joint energy functional (1) by using the d-dimensional Fourier transform (d-$\mathcal{FT}$) over the spatial variable $\mathbf{x}$, and in an efficient way if the fast algorithm for its computation (i.e., the d-FFT) is taken into account.

3.1 Application of Parseval's Theorem to the Joint Energy Functional

As a starting point, (1) has to be expressed in the frequency domain by means of Parseval's theorem, which states that the total energy contained in a signal summed across all of space is equal to the total energy of the signal's Fourier transform summed across all of its frequency components [37]. Due to the fact that digital data sets are typically encoded by uniformly distributed spatial elements in each dimension (e.g. pixels if $d=2$, or voxels if $d=3$), the discretization of the spatial variable $\mathbf{x}$ becomes a natural approach, and therefore

$$\int_{\Psi} \big|y(\mathbf{x})\big|^2 d\mathbf{x} = \frac{1}{N} \sum_{\forall n_l} \big|y[\mathbf{n}]\big|^2, \tag{13}$$

with $l=1,\ldots,d$, where $\mathbf{n}=(n_1,\ldots,n_d)^\top$ is the index of the discrete spatial position, and $N=N_1 N_2 \cdots N_d$ is the cardinal of the data sets to be registered. The application of Parseval's theorem yields the following equation:

$$\frac{1}{N} \sum_{\forall n_l} \big|y[\mathbf{n}]\big|^2 = \nu \int_{\Omega} \big|\tilde{y}(\boldsymbol{\omega})\big|^2 d\boldsymbol{\omega}, \tag{14}$$

where $\nu=((2\pi)^d N)^{-1}$ is a positive real constant, $\Omega :=]-\pi,\pi[^d$ is the d-dimensional frequency domain, $\tilde{y}$ denotes the d-dimensional Fourier transform of a signal y, and $\boldsymbol{\omega}=(\omega_1,\ldots,\omega_d)^\top$ is the d-dimensional variable in the frequency domain corresponding to the discrete spatial variable $\mathbf{n}$. Then, according to Parseval's theorem, we can compute the joint energy functional $\mathcal{J}[\mathbf{u}]$ in the frequency domain as

$$\tilde{\mathcal{J}}[\tilde{\mathbf{u}}] := \tilde{\mathcal{D}}[\tilde{R},\tilde{T};\tilde{\mathbf{u}}] + \alpha\, \tilde{\mathcal{S}}[\tilde{\mathbf{u}}], \tag{15}$$

with $\tilde{\mathbf{u}}(\boldsymbol{\omega})=(\tilde{u}_1(\boldsymbol{\omega}),\ldots,\tilde{u}_d(\boldsymbol{\omega}))^\top$, and where the distance measure $\tilde{\mathcal{D}}$ and the regularization term $\tilde{\mathcal{S}}$ are now defined in the frequency domain.

Taking into account that $(\cdot)^2=|\cdot|^2$ for real numbers, and assuming that the displacement fields we are looking for are real (i.e., $\mathbf{u}(\mathbf{x})\in\mathbb{R}^d$), we can express all the regularizers $\mathcal{S}$ considered in the spatial domain in terms of the sum of squared absolute values. Therefore (13) and (14) can be applied in order to obtain these regularization terms in the frequency domain:

1. *Elastic registration*. For this scheme, (3) can be rewritten as

$$\mathcal{S}^{\text{elas}}[\mathbf{u}] = \frac{1}{2}\int_{\Psi} \frac{\mu}{2} \sum_{l,m=1}^{d} \Big|\partial_{x_m} u_l + \partial_{x_l} u_m\Big|^2 + \lambda \Big|\sum_{l=1}^{d} \partial_{x_l} u_l\Big|^2 d\mathbf{x}. \tag{16}$$

Applying Parseval's theorem, along with the discrete approximations of the partial differential operators in the frequency domain shown in the Appendix, (16) results in

$$\tilde{\mathcal{S}}^{\text{elas}}[\tilde{\mathbf{u}}] = \frac{\nu}{2}\int_{\Omega} \frac{\mu}{2} \sum_{l,m=1}^{d} \big|\big(1-e^{-j\omega_m}\big)\tilde{u}_l + \big(1-e^{-j\omega_l}\big)\tilde{u}_m\big|^2 + \lambda \Big|\sum_{l=1}^{d}\big(1-e^{-j\omega_l}\big)\tilde{u}_l\Big|^2 d\boldsymbol{\omega}, \tag{17}$$

which can be expressed more compactly as

$$\tilde{\mathcal{S}}^{\text{elas}}[\tilde{\mathbf{u}}] = \frac{\nu}{2}\int_{\Omega} \sum_{l,m=1}^{d} \tilde{\mathcal{A}}_{lm}^{\text{elas}}(\boldsymbol{\omega})\, \tilde{u}_m\, \tilde{u}_l^*\, d\boldsymbol{\omega}, \tag{18}$$

where the operator $\tilde{\mathcal{A}}_{lm}^{\text{elas}}$ is obtained as

$$\tilde{\mathcal{A}}_{lm}^{\text{elas}}(\boldsymbol{\omega}) = \begin{cases} 2((\lambda+2\mu)(1-\cos\omega_l) + \mu\sum_{\substack{k=1\\k\neq l}}^{d}(1-\cos\omega_k)), & l=m, \\ (\lambda+\mu)\sin\omega_l \sin\omega_m, & l\neq m. \end{cases} \tag{19}$$

Note that the previous operator performs the spatial derivatives in the frequency domain, allowing for their calculation by means of products.

2. *Fluid registration*. The resulting expressions are the same as for the elastic scheme, but in this case the unknown variable is the velocity $\tilde{\mathbf{v}}(\boldsymbol{\omega})$ instead of the displacement $\tilde{\mathbf{u}}(\boldsymbol{\omega})$, i.e.,

$$\tilde{\mathcal{S}}^{\text{fluid}}[\tilde{\mathbf{u}}] = \tilde{\mathcal{S}}^{\text{elas}}[\tilde{\mathbf{v}}], \tag{20}$$

with

$$\tilde{\mathcal{A}}_{lm}^{\text{fluid}}(\boldsymbol{\omega}) = \tilde{\mathcal{A}}_{lm}^{\text{elas}}(\boldsymbol{\omega}). \tag{21}$$

In this scenario, the computation of $\mathbf{u}(\mathbf{x})$ from the velocity field $\mathbf{v}(\mathbf{x})$ is performed more efficiently in the spatial domain, because translating (5) into the frequency domain would involve periodic convolutions when computing the displacement $\tilde{\mathbf{u}}(\boldsymbol{\omega})$ from the velocity $\tilde{\mathbf{v}}(\boldsymbol{\omega})$ (although the spatial regridding, see [10], would be avoided in the frequency domain).

3. *Diffusion registration*. As in the elastic case, (6) can be rewritten as

$$\mathcal{S}^{\text{diff}}[\mathbf{u}] = \frac{1}{2}\sum_{l,m=1}^{d}\int_{\Psi}\left|\partial_{x_m}u_l\right|^2 d\mathbf{x}, \tag{22}$$

whose expression in terms of Parseval's theorem is the following:

$$\tilde{\mathcal{S}}^{\text{diff}}[\tilde{\mathbf{u}}] = \frac{\nu}{2}\sum_{l,m=1}^{d}\int_{\Omega}\left|\left(1-e^{-j\omega_m}\right)\tilde{u}_l\right|^2 d\boldsymbol{\omega}. \tag{23}$$

Finally, (23) can be reduced to

$$\tilde{\mathcal{S}}^{\text{diff}}[\tilde{\mathbf{u}}] = \frac{\nu}{2}\int_{\Omega}\tilde{\mathcal{A}}_{ll}^{\text{diff}}(\boldsymbol{\omega})\left\|\tilde{\mathbf{u}}\right\|^2 d\boldsymbol{\omega}, \tag{24}$$

where the operator $\tilde{\mathcal{A}}_{ll}^{\text{diff}}$ is defined as

$$\tilde{\mathcal{A}}_{ll}^{\text{diff}}(\boldsymbol{\omega}) = 2\sum_{m=1}^{d}\left(1-\cos\omega_m\right). \tag{25}$$

4. *Curvature registration*. As for the previous registration schemes, (7) has to be expressed in terms of sums of squared absolute values:

$$\mathcal{S}^{\text{curv}}[\mathbf{u}] = \frac{1}{2}\sum_{l=1}^{d}\int_{\Psi}\left|\sum_{m=1}^{d}\partial_{x_m x_m}u_l\right|^2 d\mathbf{x}. \tag{26}$$

After applying Parseval's theorem, (26) results in

$$\tilde{\mathcal{S}}^{\text{curv}}[\tilde{\mathbf{u}}] = \frac{\nu}{2}\sum_{l=1}^{d}\int_{\Omega}\left|\sum_{m=1}^{d}\left|1-e^{-j\omega_m}\right|^2\tilde{u}_l\right|^2 d\boldsymbol{\omega}, \tag{27}$$

which can be rewritten more compactly as

$$\tilde{\mathcal{S}}^{\text{curv}}[\tilde{\mathbf{u}}] = \frac{\nu}{2}\int_{\Omega}\tilde{\mathcal{A}}_{ll}^{\text{curv}}(\boldsymbol{\omega})\left\|\tilde{\mathbf{u}}\right\|^2 d\boldsymbol{\omega}, \tag{28}$$

where $\tilde{\mathcal{A}}_{ll}^{\text{curv}}$ is obtained as

$$\tilde{\mathcal{A}}_{ll}^{\text{curv}}(\boldsymbol{\omega}) = \left(2\sum_{m=1}^{d}\left(1-\cos\omega_m\right)\right)^2. \tag{29}$$

At this point, a general equation in the frequency domain, valid for every possible regularizing term, can be inferred from (18), (24) and (28):

$$\begin{aligned}\tilde{\mathcal{S}}[\tilde{\mathbf{u}}] &= \frac{\nu}{2}\int_{\Omega}\sum_{l,m=1}^{d}\tilde{\mathcal{A}}_{lm}(\boldsymbol{\omega})\,\tilde{u}_m\,\tilde{u}_l^*\,d\boldsymbol{\omega}\\ &= \frac{\nu}{2}\int_{\Omega}\begin{pmatrix}\tilde{u}_1 & \cdots & \tilde{u}_d\end{pmatrix}\begin{pmatrix}\tilde{\mathcal{A}}_{11}(\boldsymbol{\omega}) & \cdots & \tilde{\mathcal{A}}_{d1}(\boldsymbol{\omega})\\ \vdots & \ddots & \vdots\\ \tilde{\mathcal{A}}_{1d}(\boldsymbol{\omega}) & \cdots & \tilde{\mathcal{A}}_{dd}(\boldsymbol{\omega})\end{pmatrix}\\ &\quad\times\begin{pmatrix}\tilde{u}_1^*\\ \vdots\\ \tilde{u}_d^*\end{pmatrix}d\boldsymbol{\omega}.\end{aligned} \tag{30}$$

The previous equation can be expressed more compactly as

$$\begin{aligned}\tilde{\mathcal{S}}[\tilde{\mathbf{u}}] &= \frac{\nu}{2}\int_{\Omega}\tilde{\mathbf{u}}^{\top}\tilde{\mathcal{A}}^{\top}(\boldsymbol{\omega})\,\tilde{\mathbf{u}}^*\,d\boldsymbol{\omega}\\ &= \frac{\nu}{2}\int_{\Omega}\left\langle\tilde{\mathcal{A}}(\boldsymbol{\omega})\,\tilde{\mathbf{u}},\tilde{\mathbf{u}}\right\rangle_{\mathbb{C}^d}d\boldsymbol{\omega} := \frac{1}{2}\,\tilde{a}[\tilde{\mathbf{u}},\tilde{\mathbf{u}}],\end{aligned} \tag{31}$$

where $\langle\tilde{\mathbf{r}},\tilde{\mathbf{s}}\rangle_{\mathbb{C}^d} = \tilde{\mathbf{r}}^{\top}\tilde{\mathbf{s}}^*$ is the complex inner product in $\mathbb{C}^d$, and $\tilde{a}[\tilde{\mathbf{u}},\tilde{\mathbf{u}}]\in\mathbb{R}$ is a positive bilinear form in the frequency domain.

It should be noted that for the diffusion and curvature cases, the frequency components of the displacement field are independent and are not coupled, i.e., $\tilde{\mathcal{A}}_{lm}^{\text{diff,curv}}(\boldsymbol{\omega}) = \mathbf{0}$ (with $l\neq m$), and therefore

$$\tilde{\mathcal{A}}^{\text{diff,curv}}(\boldsymbol{\omega}) = \mathbf{I}_d\otimes\tilde{\mathcal{A}}_{ll}^{\text{diff,curv}}(\boldsymbol{\omega}), \tag{32}$$

where $\mathbf{I}_d$ is the $d\times d$ identity matrix, and $\otimes$ denotes the Kronecker product of matrices.

3.2 Design of Hybrid Diffusion-Curvature Regularizers

In some applications (e.g. in medical imaging, where the data sets typically represent different tissues), one can be interested in a registration scheme based on a regularization term with gradual stiffness properties, apart from the classical rigidity (i.e., diffusion) and elasticity (i.e., curvature) models. A composite regularizer as e.g. $\mathcal{S}[\mathbf{u}] = \frac{1}{2}\sum_{l=1}^{d}\int_{\Psi}\gamma\|\nabla u_l\|^2 + (1-\gamma)(\Delta u_l)^2 d\mathbf{x}$, with $\gamma\in[0,1]$, cannot accomplish this goal, because the results it produces are always closer to the diffusion behavior, except if $\gamma\approx 0$. With the purpose of designing the hybrid registration scheme, we propose the following smoother:

$$\begin{aligned}\mathcal{S}^{\text{hybr}}[\mathbf{u}] &:= \frac{1}{2}\sum_{l=1}^{d}\int_{\Psi}\left\langle\nabla^{\sigma}u_l,\nabla^{\sigma}u_l\right\rangle_{\mathbb{R}^d}d\mathbf{x}\\ &= \frac{1}{2}\sum_{l=1}^{d}\int_{\Psi}\left\|\nabla^{\sigma}u_l\right\|^2 d\mathbf{x},\end{aligned} \tag{33}$$

which cannot be implemented in the spatial domain if $\sigma \notin \mathbb{N}$, since the fractional power of the gradient operator makes no sense. Using the discrete approximations shown in the Appendix, (33) can be rewritten as

$$\mathcal{S}^{\text{hybr}}[\mathbf{u}] \approx \frac{1}{2}\sum_{l=1}^{d}\frac{1}{N}\sum_{\forall n_k}\left|\sum_{m=1}^{d}\overbrace{\mathrm{d}^-[n_m]*\cdots*\mathrm{d}^-[n_m]}^{\sigma\text{ -times}}*u_l\right|^2. \tag{34}$$

Note that the previous equation is once again meaningless in the spatial domain for non-integer values of σ. However, this problem can be approached within the proposed framework (i.e., from a frequency domain point of view). For doing so, Parseval's theorem has to be applied to (34), as seen in Section 3.1, therefore obtaining

$$\begin{aligned}\tilde{\mathcal{S}}^{\text{hybr}}[\tilde{\mathbf{u}}] &= \frac{\nu}{2}\sum_{l=1}^{d}\int_{\Omega}\left|\sum_{m=1}^{d}\left|1-e^{-j\omega_m}\right|^2\right|^{\sigma}\left|\tilde{u}_l\right|^2 d\boldsymbol{\omega}\\ &= \frac{\nu}{2}\int_{\Omega}\tilde{\mathcal{A}}_{ll}^{\text{hybr}}(\boldsymbol{\omega})\left\|\tilde{\mathbf{u}}\right\|^2 d\boldsymbol{\omega},\end{aligned} \tag{35}$$

where

$$\tilde{\mathcal{A}}_{ll}^{\text{hybr}}(\boldsymbol{\omega}) = \left(2\sum_{m=1}^{d}(1-\cos\omega_m)\right)^{\sigma}. \tag{36}$$

It should be noted that (25) and (29) are particular cases of (36), and therefore the smoother $\mathcal{S}^{\text{hybr}}$ can actually be seen as a generalized regularization term which allows for a registration technique which is between the diffusion and curvature cases, because it simultaneously includes partial features of both schemes if $\sigma \in]1,2[$.

Finally, the proposed regularizer can also be expressed in terms of the equation (31), taking into account that it produces a displacement field whose components are decoupled (i.e., $\tilde{\mathcal{A}}_{lm}^{\text{hybr}}(\boldsymbol{\omega}) = \mathbf{0}$, with $l \neq m$), and therefore

$$\tilde{\mathcal{A}}^{\text{hybr}}(\boldsymbol{\omega}) = \mathbf{I}_d \otimes \tilde{\mathcal{A}}_{ll}^{\text{hybr}}(\boldsymbol{\omega}). \tag{37}$$

3.3 Minimization of the Joint Energy Functional

According to the variational calculus, a necessary condition for a minimizer $\tilde{\mathbf{u}}$ of the joint energy functional (15) is that the first variation of $\tilde{\mathcal{J}}[\tilde{\mathbf{u}}]$ in any direction (also known as the *Gâteaux* derivative) vanishes for all suitable perturbations $\tilde{\mathbf{z}}$, i.e.,

$$\begin{aligned}&d\tilde{\mathcal{J}}[\tilde{\mathbf{u}};\tilde{\mathbf{z}}] = d\tilde{\mathcal{D}}[\tilde{R},\tilde{T};\tilde{\mathbf{u}};\tilde{\mathbf{z}}] + \alpha\, d\tilde{\mathcal{S}}[\tilde{\mathbf{u}};\tilde{\mathbf{z}}] = 0,\\ &\forall\,\tilde{\mathbf{z}} \in \mathbb{C}^d.\end{aligned} \tag{38}$$

For the Gâteaux derivative of $\tilde{\mathcal{D}}$, we find

$$\begin{aligned}d\tilde{\mathcal{D}}[\tilde{R},\tilde{T};\tilde{\mathbf{u}};\tilde{\mathbf{z}}] &= \lim_{\epsilon\to 0}\frac{1}{\epsilon}\left(\tilde{\mathcal{D}}[\tilde{R},\tilde{T};\tilde{\mathbf{u}}+\epsilon\,\tilde{\mathbf{z}}] - \tilde{\mathcal{D}}[\tilde{R},\tilde{T};\tilde{\mathbf{u}}]\right)\\ &= \nu\int_{\Omega}\left\langle\tilde{\mathbf{f}}(\boldsymbol{\omega}),\tilde{\mathbf{z}}\right\rangle_{\mathbb{C}^d} d\boldsymbol{\omega},\end{aligned} \tag{39}$$

where the so-called force field in the frequency domain, $\tilde{\mathbf{f}}(\boldsymbol{\omega})$, depends on the particular choice of the distance measure, $\tilde{\mathbf{f}}(\boldsymbol{\omega}) = d\text{-}\mathcal{FT}\{\nabla\mathcal{D}[R,T;\mathbf{u}]\} \in \mathbb{C}^d$.

For the Gâteaux derivative of $\tilde{\mathcal{S}}$, the following expression is obtained:

$$\begin{aligned}d\tilde{\mathcal{S}}[\tilde{\mathbf{u}};\tilde{\mathbf{z}}] &= \lim_{\epsilon\to 0}\frac{1}{2\epsilon}\left(\tilde{a}[\tilde{\mathbf{u}}+\epsilon\,\tilde{\mathbf{z}},\tilde{\mathbf{u}}+\epsilon\,\tilde{\mathbf{z}}] - \tilde{a}[\tilde{\mathbf{u}},\tilde{\mathbf{u}}]\right)\\ &= \tilde{a}[\tilde{\mathbf{u}},\tilde{\mathbf{z}}] = \nu\int_{\Omega}\left\langle\tilde{\mathcal{A}}(\boldsymbol{\omega})\,\tilde{\mathbf{u}},\tilde{\mathbf{z}}\right\rangle_{\mathbb{C}^d} d\boldsymbol{\omega},\end{aligned} \tag{40}$$

where (31) has been used. Note that any energy-based smoother $\tilde{\mathcal{S}}$ can be incorporated into this framework, as long as it can be expressed in terms of (31).

Finally, we can write (38) as

$$\begin{aligned}d\tilde{\mathcal{J}}[\tilde{\mathbf{u}};\tilde{\mathbf{z}}] &= \nu\int_{\Omega}\left\langle\tilde{\mathbf{f}}(\boldsymbol{\omega}) + \alpha\,\tilde{\mathcal{A}}(\boldsymbol{\omega})\,\tilde{\mathbf{u}},\tilde{\mathbf{z}}\right\rangle_{\mathbb{C}^d} d\boldsymbol{\omega}\\ &= 0, \quad \forall\,\tilde{\mathbf{z}} \in \mathbb{C}^d,\end{aligned} \tag{41}$$

which leads to the Euler-Lagrange equation in the frequency domain:

$$\tilde{\mathbf{f}}(\boldsymbol{\omega}) + \alpha\,\tilde{\mathcal{A}}(\boldsymbol{\omega})\,\tilde{\mathbf{u}}(\boldsymbol{\omega}) = \mathbf{0}. \tag{42}$$

Solving the previous equation in the frequency domain provides a stable implementation for the computation of a numerical solution for the displacement field, and in a more efficient way than existing approaches if the multidimensional fast Fourier transform (d-FFT) is used. In the following section we will also see that the proposed framework allows to understand the regularization forces as a d-dimensional low-pass filtering of the displacement field $\mathbf{u}(\mathbf{x})$, which can be obtained as the inverse Fourier transform of $\tilde{\mathbf{u}}(\boldsymbol{\omega})$.

4 Frequency Implementation of the Euler-Lagrange Equations

To solve the Euler-Lagrange equations (42) formulated in the frequency domain, a fixed-point or time-marching scheme can be employed. The fixed-point scheme yields the following iteration:

$$\tilde{\mathbf{u}}^{(\xi)}(\boldsymbol{\omega}) = \left(\alpha\,\tilde{\mathcal{A}}(\boldsymbol{\omega})\right)^{-1}\left(-\tilde{\mathbf{f}}^{(\xi-1)}(\boldsymbol{\omega})\right), \tag{43}$$

being $\xi \in \mathbb{N}$ the iteration index. The inversion of matrix $\tilde{\mathcal{A}}(\boldsymbol{\omega})$ has to be made carefully because it is ill-conditioned and in its inversion a division by zero occurs. An alternative strategy like Moore-Penrose pseudo-inverse (or like Drazin generalized inverse) has to be taken into account for avoiding an unstable behavior [4].

Using a time-marching scheme to solve (42) gives rise to the equation

$$\partial_t \tilde{\mathbf{u}}(\boldsymbol{\omega}, t) + \tilde{\mathbf{f}}(\boldsymbol{\omega}, t) + \alpha\, \tilde{\mathcal{A}}(\boldsymbol{\omega})\, \tilde{\mathbf{u}}(\boldsymbol{\omega}, t) = \mathbf{0}\,, \tag{44}$$

where $\partial_t \tilde{\mathbf{u}}(\boldsymbol{\omega}, t) = (\partial_t \tilde{u}_1(\boldsymbol{\omega}, t), \ldots, \partial_t \tilde{u}_d(\boldsymbol{\omega}, t))^\top$ (in the steady-state $\partial_t \tilde{\mathbf{u}}(\boldsymbol{\omega}, t) = \mathbf{0}$ and (44) holds (42)). In order to solve (44), the time t is discretized, $t := \xi\, \tau$, being $\tau > 0$ the time-step, and the time derivative of $\tilde{\mathbf{u}}(\boldsymbol{\omega}, t)$ is replaced by its discrete approximation (first backward difference):

$$\partial_t \tilde{\mathbf{u}}(\boldsymbol{\omega}, t) \approx \big(\tilde{\mathbf{u}}(\boldsymbol{\omega}, \xi\, \tau) - \tilde{\mathbf{u}}(\boldsymbol{\omega}, \xi\, \tau - \tau)\big)/\tau\,. \tag{45}$$

Using the notation $\tilde{\mathbf{u}}^{(\xi)}(\boldsymbol{\omega}) := \tilde{\mathbf{u}}(\boldsymbol{\omega}, \xi\tau)$, the resulting iteration is the following:

$$\begin{aligned}\tilde{\mathbf{u}}^{(\xi)}(\boldsymbol{\omega}) = {} & \big(\mathbf{I} + \tau\, \alpha\, \tilde{\mathcal{A}}(\boldsymbol{\omega})\big)^{-1} \\ & \times \big(\tilde{\mathbf{u}}^{(\xi-1)}(\boldsymbol{\omega}) - \tau\, \tilde{\mathbf{f}}^{(\xi-1)}(\boldsymbol{\omega})\big),\end{aligned} \tag{46}$$

where $\mathbf{I}$ denotes the identity on the domain Ω, and where $\tilde{\mathbf{u}}^{(\xi)}(\boldsymbol{\omega})$ is usually initialized to zero, $\tilde{\mathbf{u}}^{(0)}(\boldsymbol{\omega}) := \mathbf{0}$. The previous scheme can be understood as the (globally convergent) steepest descent method, where the identity matrix is added to the Hessian (which is equivalent to $\alpha\, \tilde{\mathcal{A}}$ in our implementation) in order to make it positive definite, and therefore the existence and uniqueness of the solution is guaranteed.[2]

4.1 Registration Methods with Decoupled Components

In the case of diffusion, curvature, and the proposed hybrid approach, the frequency components of the displacement field are independent (i.e., they are not coupled), and then matrix $\tilde{\mathcal{A}}(\boldsymbol{\omega})$ can be written as shown in (32) and (37). In these cases, the matrix inversion in (46) does disappear due to the fact that the multiplication of a circulant block matrix and a column block vector becomes a Hadamard (i.e., pointwise) product of their respective spectra in the frequency domain [14]. Then, the iteration for the l-th component is given by

$$\tilde{u}_l^{(\xi)}(\boldsymbol{\omega}) = \frac{1}{1 + \tau\, \alpha\, \tilde{\mathcal{A}}_{ll}(\boldsymbol{\omega})} \big(\tilde{u}_l^{(\xi-1)}(\boldsymbol{\omega}) - \tau\, \tilde{f}_l^{(\xi-1)}(\boldsymbol{\omega})\big). \tag{47}$$

For the purpose of writing the previous equation more compactly, the following variables are defined:

$$\begin{aligned}&\eta := 1/\tau, \\ &K(\boldsymbol{\omega}) := \alpha\, \tilde{\mathcal{A}}_{ll}(\boldsymbol{\omega}), \\ &H(\boldsymbol{\omega}) := \frac{\eta}{\eta + K(\boldsymbol{\omega})}.\end{aligned} \tag{48}$$

[2]The addition of a correction matrix is a useful strategy for improving the stability and computational efficiency of optimization algorithms such as conjugated gradient (CG) or Newton-type methods.

$H(\boldsymbol{\omega})$ is a d-dimensional low-pass filter, it has its maximum at the frequencies of the DC component. The values of $H(\boldsymbol{\omega})$ are less or equal than one and are the reciprocal of $1 + \eta^{-1} K(\boldsymbol{\omega})$, therefore the matrix inversion necessary for solving (46) has become a pointwise division. $H(\boldsymbol{\omega})$ is then the pseudo-inverse filter of $K(\boldsymbol{\omega})$, which corresponds to a d-dimensional high-pass filter that contains the frequency representation of the spatial derivatives, and the constant η is related to the width of the transition band of filter $H(\boldsymbol{\omega})$.

Finally, the equation that expresses the evolution of the l-th component of the displacement field is the following:

$$\tilde{u}_l^{(\xi)}(\boldsymbol{\omega}) = H(\boldsymbol{\omega})\big(\tilde{u}_l^{(\xi-1)}(\boldsymbol{\omega}) - \eta^{-1}\, \tilde{f}_l^{(\xi-1)}(\boldsymbol{\omega})\big)\,. \tag{49}$$

The frequency point of view allows to understand the internal forces, with the restrictions imposed on the displacement field by the regularizer, as a low-pass filtering. In (49), each component of the displacement field as well as the driving external forces, weighted by the value η^{-1}, are low-pass filtered. Figure 1 depicts the frequency spectra of filters $H(\boldsymbol{\omega})$ for the diffusion, curvature and hybrid cases. Filter $H(\boldsymbol{\omega})$ for curvature registration (Fig. 1(c)) shows a wider pass-band and a narrower transition band than filter $H(\boldsymbol{\omega})$ for diffusion registration (Fig. 1(a)). As expected, filters obtained with the hybrid approach show an intermediate behavior between the diffusion and curvature cases, see Fig. 1(b) and Fig. 1(d). The smoothness of the resulting displacement field depends on the pass-bandwidth of the low-pass filter, which is usually measured by the cut-off frequency (defined as $\omega_c : |H(\omega > \omega_c)| < 1/\sqrt{2}$) or by Bode's corner frequency (defined as the frequency where the two asymptotic lines of the magnitude Bode plot meet). The pass-bandwidth is higher for curvature than for diffusion and it is related to the order of the derivative which is being minimized, see Fig. 1(e) and Fig. 1(f); the cut-off angular frequency (in radians) can be approximated by means of a quadratic polynomial fitting as $\omega_c \approx -0.093\,\sigma^2 + 0.45\,\sigma + 0.31$, and Bode's corner angular frequency (in radians) can be computed as $\omega_B \approx 0.46\,\sigma^3 - 2.66\,\sigma^2 + 5.4\,\sigma - 3.18$. Moreover, we can choose the value of the regularization order from a known value of the cut-off frequency or the corner frequency as $\sigma \approx 19.43\,\omega_c^2 - 23.03\,\omega_c + 7.76$ and $\sigma \approx 3.39\,\omega_B^3 - 1.53\,\omega_B^2 + \omega_B + 0.99$, respectively. It should be noted that the latter study, for the case $\sigma \notin [1, 2]$ (e.g., higher-order regularizers), is out of the scope of this paper.

In terms of the registration results, a higher regularization order provides a higher pass-bandwidth, and then the spatial resolution is higher; in other words, a higher σ means more variations (i.e., higher frequencies) in the displacement field, therefore obtaining more flexible transformations and allowing for faster convergence times. On the other hand, a lower regularization order provides a lower pass-bandwidth, and then the influence of each computed vector "propagates"

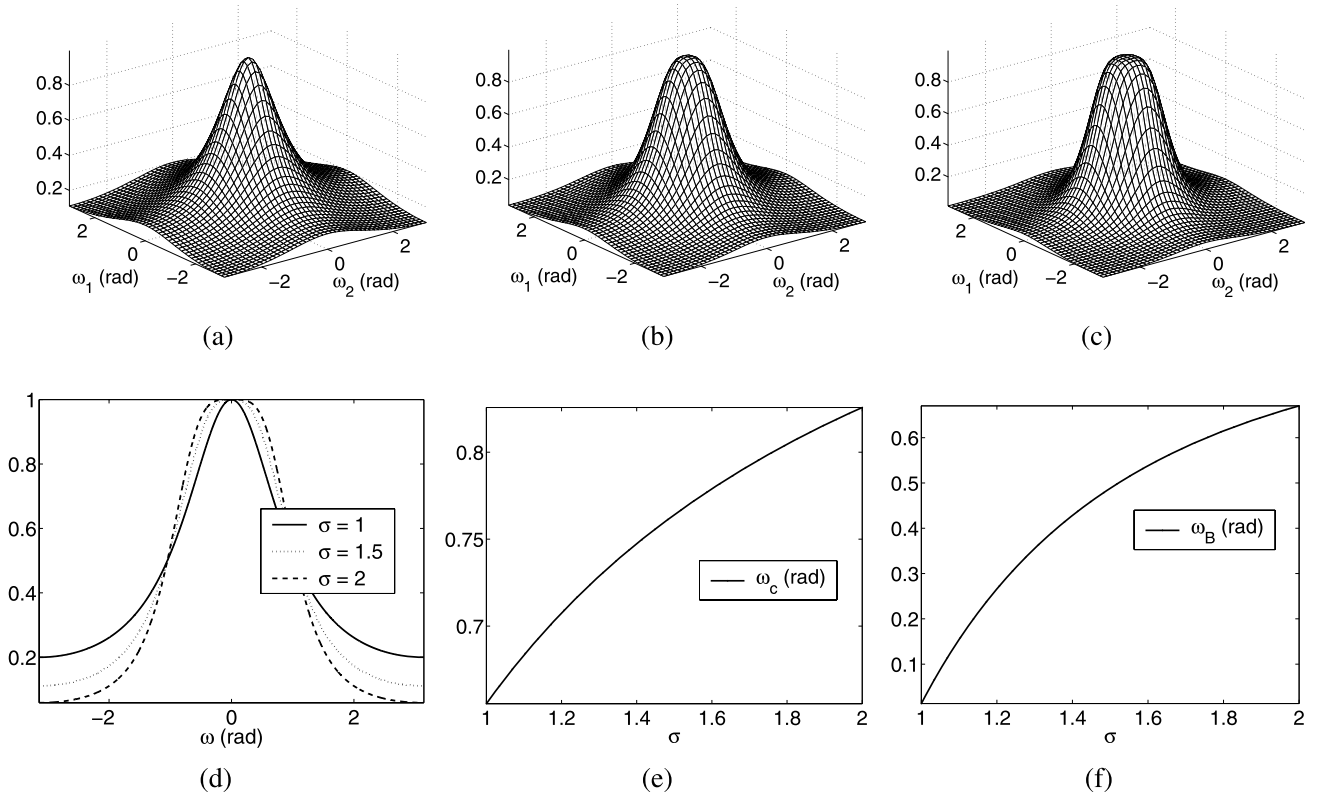

Fig. 1 Spectra of d-dimensional filters, $d = 2$, $\eta = 1$, $\alpha = 1$. (**a**) $H(\boldsymbol{\omega})$ for diffusion, (**b**) $H(\boldsymbol{\omega})$ for $\sigma = 1.5$, (**c**) $H(\boldsymbol{\omega})$ for curvature, (**d**) Comparison of the frequency responses, (**e**) Effect of the regularization order σ in the cut-off frequency ω_c, (**f**) Effect of the regularization order σ in Bode's corner frequency ω_B

farther in space; in other words, a lower σ means less variations in $\mathbf{u}(\mathbf{x})$, and therefore the resulting displacement field is more uniform and it presents less oscillations (although some transformations, like rotations, would not be allowed in this case).

4.2 Efficiency Comparison

For the elastic and fluid registration techniques, direct solution schemes in the spatial domain are available [36]. However, these schemes require, for $N_1 \times \cdots \times N_d$ data sets, the inversion of an ill-conditioned, sparse matrix of size $d\,N \times d\,N$, where $N = N_1\,N_2 \cdots N_d$ is the cardinal of the data sets to be registered, and therefore they are not suitable for typical registration scenarios, since the computer runs out of memory. Even fast schemes based on a singular value decomposition (SVD) (see e.g. [15]) require the (pseudo-) inversion of d^2 matrices of size $N_1 \times \cdots \times N_d$, which can be very time-consuming. For these registration techniques there is no noticeable improvement in efficiency if the proposed frequency implementation is used.

Direct solution schemes in the spatial domain are also available for the diffusion and curvature registration techniques [36]. In these cases, a matrix of size $N \times N$ has to be inverted. There exists the possibility of fast implementations based on a DCT-type factorization [20], without any matrix inversion involved in the procedure. Alternative approaches based on multigrid and/or multiscale techniques offer stable and robust implementations for all four considered registration methods, but they demand a Cholesky factorization with high computational complexity, thus conditioning the overall performance of the resulting algorithms, as already commented at the end of Sect. 2. Particularly, for the diffusion registration technique, an efficient implementation based on an additive operator splitting (AOS) scheme is also available [16], but it is outperformed by previously referred DCT-based scheme, which is faster due to both the complexity of the preprocessing stage required by the AOS implementation and the excellent implementation of the DCT routine provided by many programming languages (e.g. MATLAB, C/C++): the DCT functions are based on the library FFTW [21]. Therefore, in terms of efficiency, the only relevant comparison is the DCT-based scheme (which is included e.g. in the FLIRT toolbox [19, 38]) versus the proposed frequency domain implementation, for the diffusion or curvature registration scenarios, since both registration techniques are identical in terms of complexity (see Sects. 3.1 and 4.1). Finally, it should be

Table 1 Mean timings in seconds and ratios for one iteration of the most efficient spatial domain implementation (DCT-based) and the proposed frequency domain implementation

Size of data sets	Spatial domain implem. timings	Frequency domain implem. timings	Actual ratio
256×256	0.127	0.053	2.39
512×512	1.063	0.449	2.37
1024×1024	4.303	1.844	2.33
$64 \times 64 \times 64$	1.698	0.729	2.33
$128 \times 128 \times 128$	15.185	5.959	2.55

noted that the frequency approach is the most straightforward way for the implementation of the hybrid scheme proposed in Sect. 3.2, because the fractional power of the gradient operator cannot be easily computed in the spatial domain.

Table 1 shows the timings for one iteration of the registration algorithm (i.e., for the solution of one linear system of equations arising in a generic variational image registration scenario), as well as the actual ratios between the timings of the implementations under discussion (with $d = 2$ and $d = 3$); the proposed frequency domain-based scheme is more than two times faster than the fastest implementation available in the spatial domain. These timings were obtained on a PC with Intel Pentium IV, 2.8 GHz, 512 MByte RAM, and the computations were performed under MATLAB 6.5 (R13). Note that the complexity of a d-DCT of size $N_1 \times \cdots \times N_d$ is approximately twice the complexity of a d-FFT of the same size. Then the estimation of the complexity of one iteration of the registration algorithm, without considering the warping of the template image with the computed partial mapping, is $\mathcal{O}(4\,d\,N \log_2 N)$ for the DCT-based scheme (where d d-DCT, d d-IDCT and dN additional products are performed), and $\mathcal{O}(2\,d\,N \log_2 N)$ for the proposed frequency domain implementation (where d d-FFT, d d-IFFT and dN additional products are performed), and therefore the theoretical ratio between the timings is $\rho \approx 2$. It is assumed that the complexity of a FFT is $\mathcal{O}(N \log_2 N)$ [37], taking into account that both the d-FFT and the d-DCT are internally implemented as separable transforms, i.e., the computation of a d-dimensional FFT (DCT) involves N_l $(d\text{-}1)$-dimensional FFTs (DCTs) and N/N_l one-dimensional FFTs (DCTs).

In summary, the overall complexity of the proposed registration method is $\mathcal{O}(N \log_2 N)$. The preprocessing stage (where the N values of $H(\boldsymbol{\omega})$ are computed) has a complexity of $\mathcal{O}(N)$. During each iteration, we can distinguish three procedures: the computation of the external forces, $\mathbf{f}(\mathbf{x}; \mathbf{u})$, which depend on the particular distance term chosen, having in all cases a complexity of $\mathcal{O}(N)$; the computation of the displacement field, $\mathbf{u}(\mathbf{x})$, which has a complexity of $\mathcal{O}(2\,d\,N \log_2 N)$; and the computation of the deformed template, $T_{\mathbf{u}}$, which depends on the particular choice of the interpolation scheme (in this paper, we make use of d-linear interpolation [36], since it achieves a good trade-off between complexity, $\mathcal{O}(N)$, and accuracy). Therefore the global complexity, considering ξ_{max} iterations of the registration algorithm, is

$$\mathcal{O}(N) + (\mathcal{O}(N) + \mathcal{O}(2\,d\,N \log_2 N) + \mathcal{O}(N))\,\xi_{max} \approx \mathcal{O}(N \log_2 N). \tag{50}$$

5 Registration Results

In this section, the proposed frequency domain framework is tested on two experiments involving three-dimensional ($d = 3$) data sets. In both cases, iteration (46) is performed as long as the distance measure is a decreasing sequence, i.e., while $\tilde{\mathcal{D}}[\tilde{R}, \tilde{T}; \tilde{\mathbf{u}}^{(\xi)}] < \tilde{\mathcal{D}}[\tilde{R}, \tilde{T}; \tilde{\mathbf{u}}^{(\xi-1)}]$, or until the condition $\tilde{\mathbf{f}}(\boldsymbol{\omega}; \tilde{\mathbf{u}}^{(\xi)}) \approx \mathbf{0}$ is satisfied. The distance metric and the simulation parameters are explicitly specified for each experiment.

We use simulated deformations over real data to evaluate our method first. A randomly selected magnetic resonance (MR-T1) volume of a human head (109 axial slices of size 256×256 pixels), obtained from [39], is synthetically warped using a known grid transformation. The grid transformation is a uniform periodic one in order to compare the recovery over the whole area of the data set. The deformation we adopt is $u_l(\mathbf{x}) = 5\cos(x_l\,\pi/32)$. The reference and template volumes are shown in the first and second column, respectively, of Fig. 2. To assess the validity of the proposed formulation, convenient quantitative measures are chosen: the peak signal-to-noise ratio (defined as $\text{PSNR} = 20\log_{10}(255/\text{RMSE})$, where RMSE is the root mean squared error between the data sets), the mutual information (MI) and the correlation ratio (CR). Before the registration process, the values for these measures are PSNR = 21.1 dB, MI = 0.43, and CR = 50.3%, respectively. For the PSNR measure, an improvement of 0.5 dB becomes visible, and a value higher than 30 dB is usually considered a good match of the data sets; for the CR, a value of 100% implies a perfect match of the data sets; for the MI, such thresholds are not available, and therefore a related measure such as the normalized mutual information (NMI, constrained to the interval $[1, 2]$) or the entropy correlation coefficient (ECC, constrained to the interval $[0, 1]$) should be taken into account. After the registration procedure, the computed values are PSNR = 33.3 dB, MI = 0.99, and CR = 96.6%,

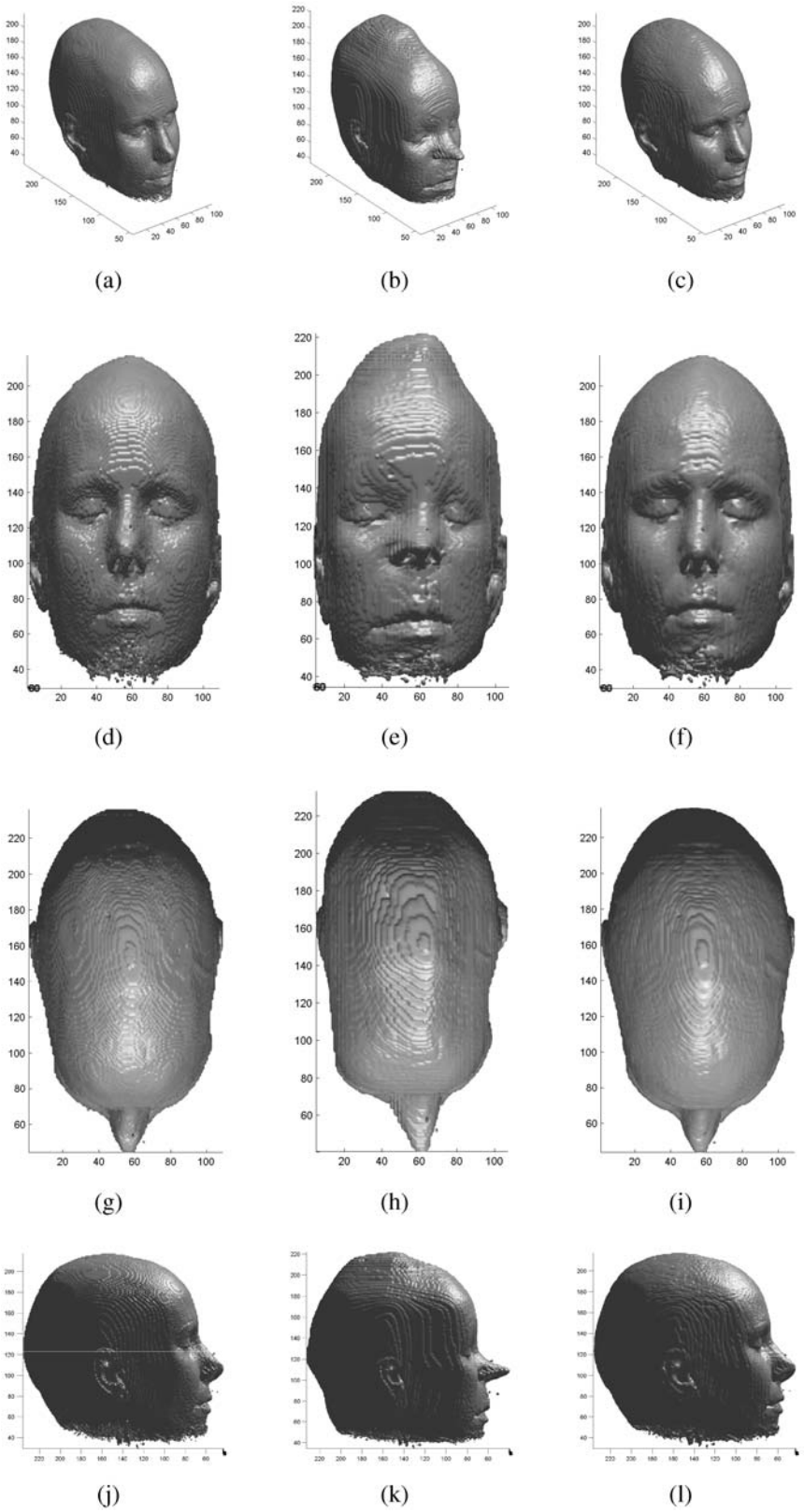

Fig. 2 Registration of a synthetically warped volume of a human head. *First column*: views of the reference data set. *Second column*: views of the template data set. *Third column*: views of the registered template. *First row*: 3D views. *Second row*: front views. *Third row*: top views. *Fourth row*: side views

respectively. Table 2 shows the values of these measures for the particular slices displayed in Fig. 3. The distance measure chosen for the registration is the sum of squared differences (SSD), the selected smoothing term

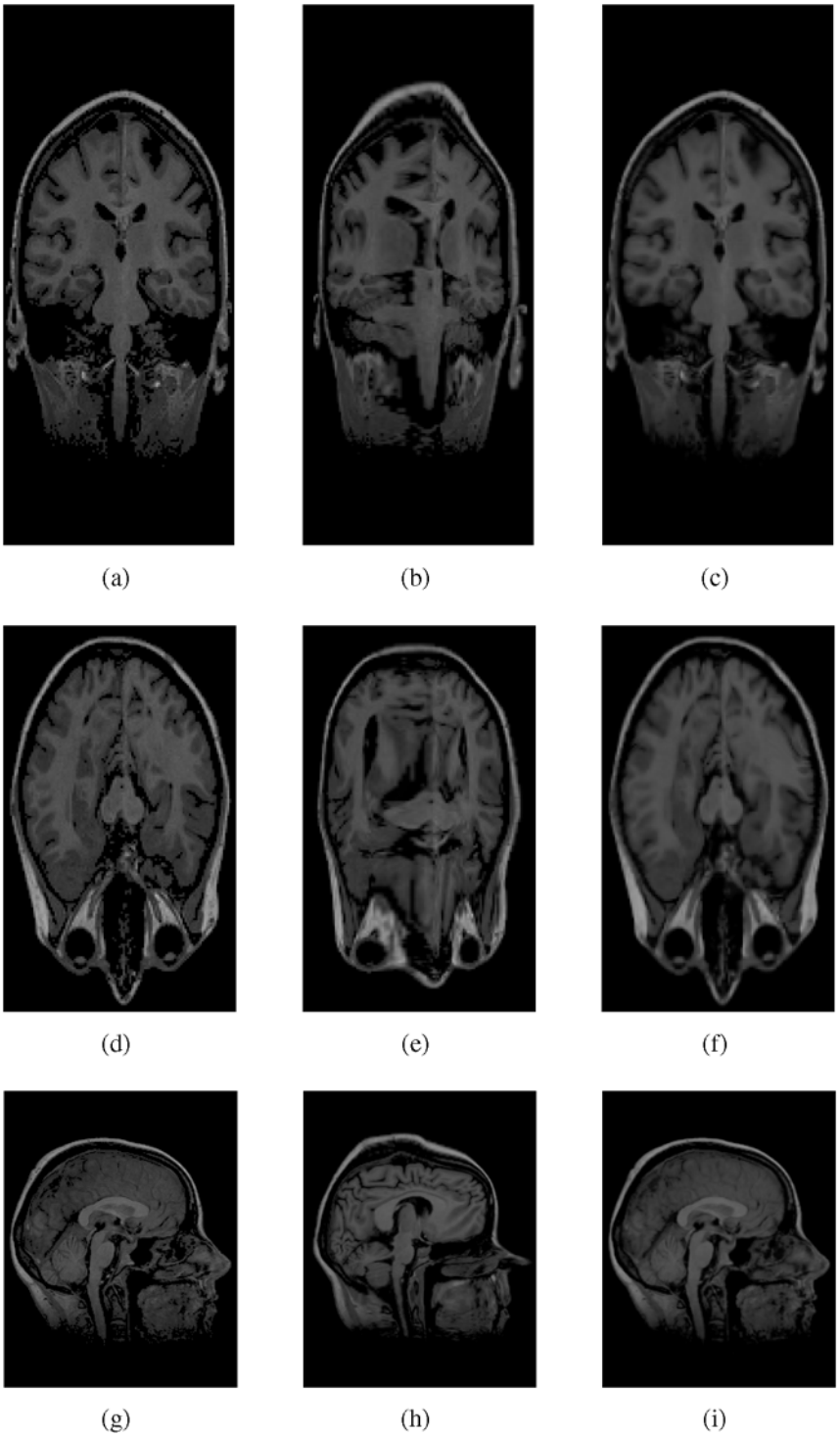

Fig. 3 Registration of a synthetically warped volume of a human head. *First column*: slices of the reference data set. *Second column*: slices of the template data set. *Third column*: slices of the registered template. *First row*: coronal slices (slice #80). *Second row*: axial slices (slice #64). *Third row*: sagittal slices (slice #28)

is the diffusion regularizer (see (24)), and the simulation parameters are $\alpha = 10$ (regularization parameter[3]) and $\eta = 1$ (reciprocal of the time-step, see (48)). If compared with the results obtained with the DCT-based spatial domain implementation (using the same simulation parameters), we can conclude that the registration results provided by both schemes are almost identical: the RMSE

[3]In the experiments shown in this paper (where a diffusion registration and a curvature registration are performed), the regularization parameter α is obtained in each case empirically, as a high enough value which guarantees a reasonable deformation of the template (i.e., not an arbitrary and unlikely one).

Table 2 Registration of a synthetically warped volume of a human head

Slices	PSNR	MI	CR
Coronal (before registration)	18.5 dB	0.65	39.3%
Coronal (after registration)	30.2 dB	1.59	95.1%
Axial (before registration)	17.5 dB	0.71	34.4%
Axial (after registration)	30.6 dB	1.61	96.1%
Sagittal (before registration)	20.2 dB	0.58	46.5%
Sagittal (after registration)	32.5 dB	1.34	96.1%

Table 3 Registration of CT and PET volumes of a human body

Slices	PSNR	MI	CR
Coronal (before registration)	N/A	1.13	22.3%
Coronal (after registration)	N/A	1.91	60.9%
Axial (before registration)	N/A	0.35	32.9%
Axial (after registration)	N/A	0.81	70.6%
Sagittal (before registration)	N/A	1.12	40.5%
Sagittal (after registration)	N/A	1.73	69.3%

and the CR between the registered templates of the considered implementations are respectively RMSE = 1.534 (i.e., the PSNR is 44.4 dB), and CR = 99.3%. Apart from the registration timings (the proposed implementation is two times faster, as discussed in Sect. 4.2), the only difference can be found in the boundary of the registered data sets, since spatial domain-based schemes impose Von Neumann boundary conditions, and the frequency domain-based scheme imposes periodic boundary conditions (actually, due to the use of the d-dimensional discrete Fourier transform, periodic boundary conditions arise naturally when computing a numerical solution for the displacement field). Anyway, when dealing with medical images, where the information is typically contained within a uniform background, this difference is hardly noticeable, as has been previously stated by other authors, see e.g. [15].

To demonstrate the performance of the proposed framework in registering actual clinical data, we use a set of 57 corresponding image pairs (axial slices of size 128×128 pixels) from a computed tomography (CT) and a positron emission tomography (PET) of a human body, obtained from [1]. Due to the differences in acquisition protocols for CT and PET, there is an inherent non-linear mismatch between the anatomic and physiologic representations of the thorax and abdomen seen in these two scans, respectively (Figs. 4 and 5). As a result, this experiment presents a good challenge to test the ability of the algorithm to handle actual multimodal clinical data. The CT volume is considered the reference data set and the PET volume is treated as the template data set to be transformed to match the CT volume. The resulting scenario belongs to the so-called intra-subject registration case. The chosen distance measure for the registration is in this case the mutual information (see e.g. [13]), the considered regularizer is the curvature term (28), and the simulation parameters are $\alpha = 10^5$ and $\eta = 1$. In this experiment, the validation is based only on the statistical measures (MI and CR). The PSNR becomes useless in this case, since the volumes to be registered do not share the same intensity levels. The mutual information and the correlation ratio computed over the original data sets are MI = 0.21 and CR = 26.4%, respectively. After the registration procedure, the new values are MI = 0.51 and CR = 65.4%, respectively. Table 3 shows the values of these quantitative measures for the particular slices displayed in Fig. 5. It should be noted that the correlation ratio, although high, cannot present a value close to 100%, because in this case the data sets do not contain exactly the same information (since they are obtained from different modalities), and therefore achieving a perfect match is not possible. Finally, the numerical difference between the registered templates for the spatial domain-based and the frequency domain-based implementations is only RMSE = 1.581 (i.e., the PSNR is 44.2 dB). Therefore the results provided by these two schemes are almost identical: the CR between both registered templates is CR = 98.7% but, as expected, the proposed FFT-based implementation allows for (two times) faster registration timings, see Sect. 4.2.

6 Conclusion

In this paper, a framework defined in the frequency domain is proposed for approaching the variational image registration problem. The joint energy functional $\mathcal{J}$ is translated into the frequency domain by means of Parseval's theorem, and the minimization of the resulting variational equations is performed entirely in this domain. This approach allows to understand the regularization constraints (or internal forces) as a low-pass filtering of the displacement field. The internal forces are derived from the regularizer and lead to the elastic, fluid, diffusion and curvature (or even *hybrid*) registration schemes in the frequency domain.

The novel formulation allows for an implementation of the registration methods more efficient than existing approaches. The use of the frequency domain (especially if the d-FFT is taken into account) reduces considerably the numerical complexity and memory requirements of the overall iterative schemes. In particular, for the popular *diffusion* and *curvature* registration approaches, the proposed framework provides a $\mathcal{O}(2\,d\,N\log_2 N)$ implementation, where N denotes the cardinal of the data sets to be registered, thus becoming efficient and fast variational registration techniques. Furthermore, the frequency-based implementation could be

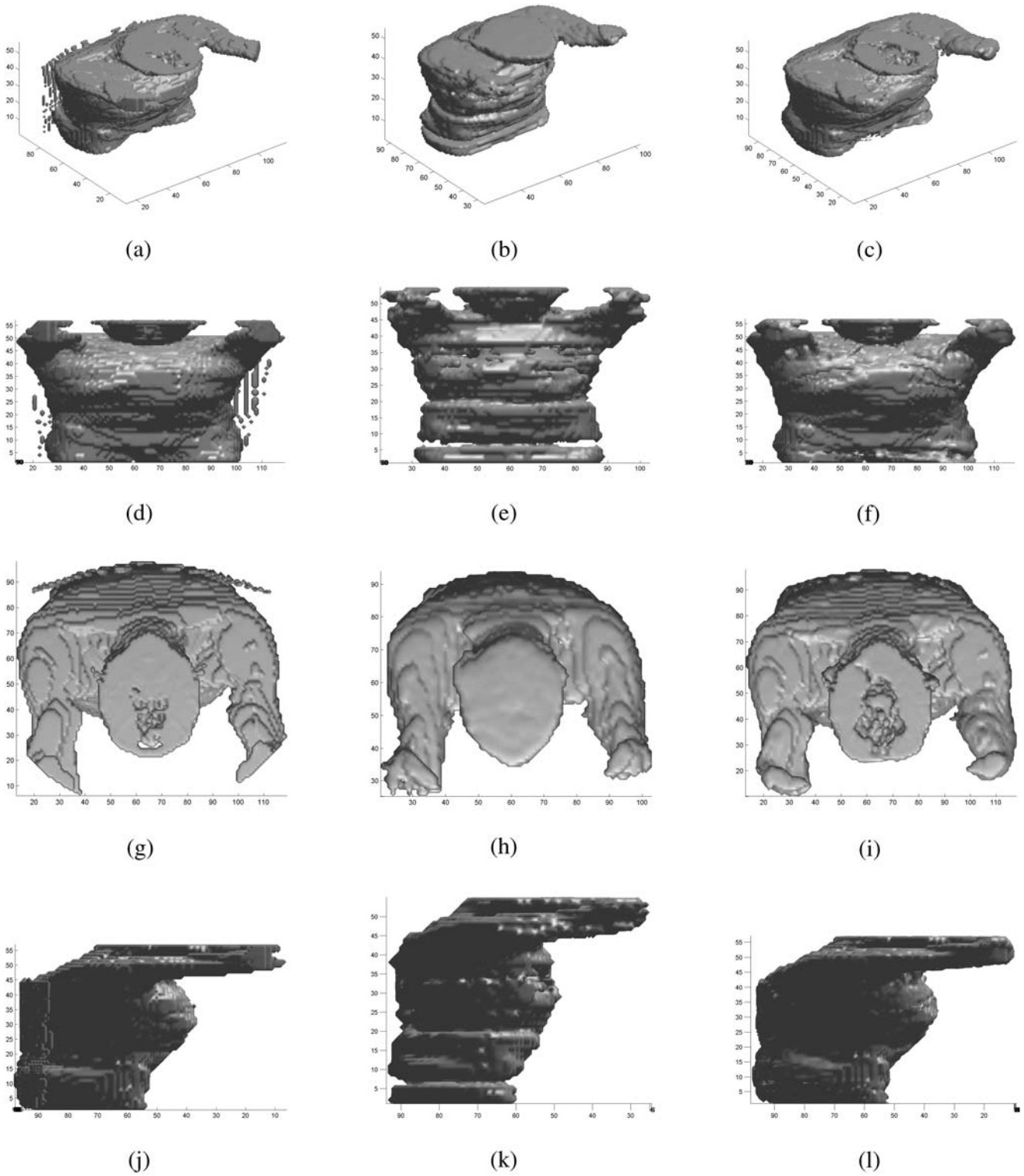

Fig. 4 Registration of CT and PET volumes of a human body. *First column*: views of the reference data set. *Second column*: views of the template data set. *Third column*: views of the registered template. *First row*: 3D views. *Second row*: front views. *Third row*: top views. *Fourth row*: side views

easily used in conjunction with a multigrid and/or multiscale approach to yield an even better convergence rate. As an example of the use of the proposed method along with a multiscale approach, the registration process can be started with

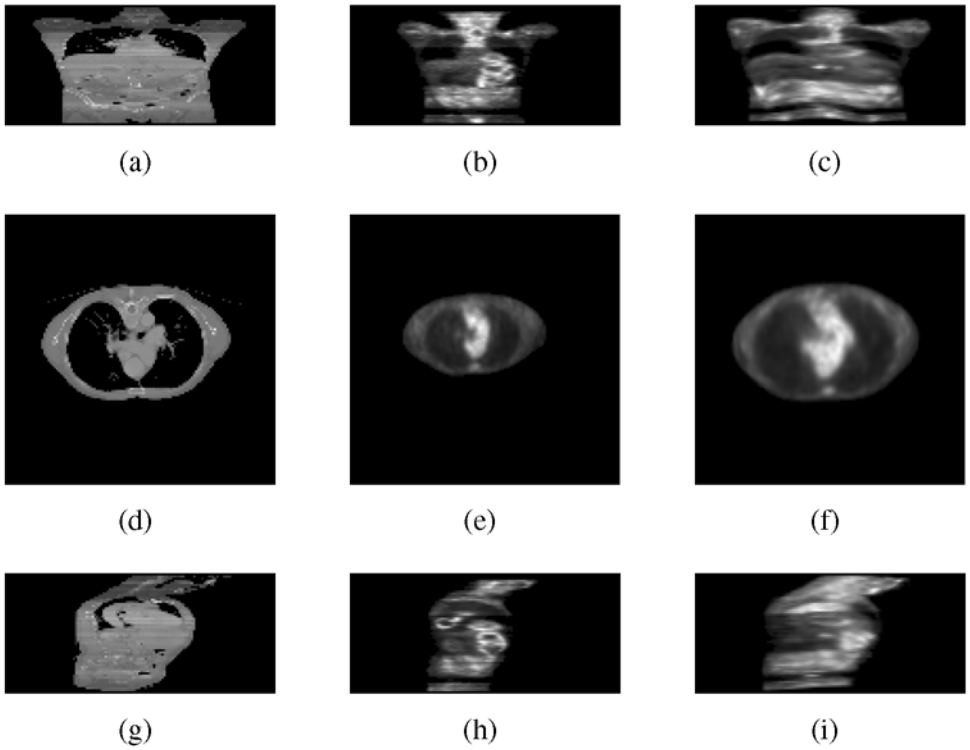

Fig. 5 Registration of CT and PET volumes of a human body. *First column*: slices of the reference data set. *Second column*: slices of the template data set. *Third column*: slices of the registered template. *First row*: coronal slices (slice #64). *Second row*: axial slices (slice #40). *Third row*: sagittal slices (slice #69)

a low value of η, thus obtaining a fast but "coarse" registration (because only low frequencies are allowed in the displacement field), which means an excellent starting point; after a few iterations (i.e., with each new *scale*), a higher value of the parameter η is used (thus allowing higher frequencies), and this way only minimum corrections (which means a low number of iterations) have to be computed over the matching vectors obtained in the previous scale. On the other hand, a multigrid strategy can also be added to the proposed implementation, by performing a previous hierarchical (or pyramidal) decomposition of the original data sets and then a coarse-to-fine sequential (or "cascade" computation of the registration step (with complexity $\mathcal{O}(N \log_2 N)$) in each image resolution (i.e., the coarse resolution transformation is prolongated onto the next finer grid, where one expects lower computational costs for corrections).

Appendix

In order to compute the discrete approximations for the partial differential operators arising in a d-dimensional registration scenario, the following operators are defined:

$$\mathrm{d}^-[n] := \delta[n] - \delta[n-1],$$

$$\mathrm{d}^+[n] := \delta[n+1] - \delta[n],$$

$$\mathrm{d}^{\mathrm{c}}[n] := \left(\mathrm{d}^-[n] + \mathrm{d}^+[n]\right)/2,$$

$$\mathrm{d}^2[n] := \mathrm{d}^-[n] * \mathrm{d}^+[n],$$

where d^-, d^+, d^{c} and d^2 perform the backward difference, forward difference, central difference and second order difference, respectively, δ is the Kronecker delta and $*$ denotes the linear convolution. Then, the discrete approximations for the first and second order spatial derivatives are the following:

$$\partial_{x_l} u(\mathbf{x}) \approx \mathrm{d}^-[n_l] * u[\mathbf{n}],$$

$$\partial_{x_l x_l} u(\mathbf{x}) \approx \mathrm{d}^2[n_l] * u[\mathbf{n}],$$

$$\partial_{x_l x_m} u(\mathbf{x}) \approx \mathrm{d}^{\mathrm{c}}[n_l] * \mathrm{d}^{\mathrm{c}}[n_m] * u[\mathbf{n}].$$

Using the previous discrete approximations, the partial differential operators can be described by the following equations:

$$\nabla \mathbf{u}(\mathbf{x}) = \left(\partial_{x_m} u_l(\mathbf{x})\right)_{l,m=1,\ldots,d} \approx \left(\mathrm{d}^-[n_m] * u_l[\mathbf{n}]\right)_{l,m=1,\ldots,d} \in \mathbb{R}^{d\times d},$$

$$\operatorname{div} \mathbf{u}(\mathbf{x}) = \sum_{l=1}^{d} \partial_{x_l} u_l(\mathbf{x}) \approx \sum_{l=1}^{d} \mathrm{d}^-[n_l] * u_l[\mathbf{n}] \in \mathbb{R},$$

$$\Delta \mathbf{u}(\mathbf{x}) = \left(\sum_{m=1}^{d} \partial_{x_m x_m} u_l(\mathbf{x})\right)_{l=1,\ldots,d} \approx \left(\sum_{m=1}^{d} \mathrm{d}^2[n_m] * u_l[\mathbf{n}]\right)_{l=1,\ldots,d} \in \mathbb{R}^d.$$

At this point, in order to find the expressions for the previous operators in the frequency domain, it should be noted that the Fourier transform of the spatial sequence $y[n] = \delta[n - n_0]$ is $\tilde{y}(\omega) = e^{-j\omega n_0}$ [37], and therefore the following equations are obtained:

$$\mathcal{FT}\{\nabla \mathbf{u}(\mathbf{x})\} \approx \left(\left(1 - e^{-j\omega_m}\right)\tilde{u}_l(\boldsymbol{\omega})\right)_{l,m=1,\ldots,d} \in \mathbb{C}^{d\times d},$$

$$\mathcal{FT}\{\operatorname{div} \mathbf{u}(\mathbf{x})\} \approx \sum_{l=1}^{d}\left(1 - e^{-j\omega_l}\right)\tilde{u}_l(\boldsymbol{\omega}) \in \mathbb{C},$$

$$\mathcal{FT}\{\Delta \mathbf{u}(\mathbf{x})\} \approx \left(-\sum_{m=1}^{d}\left|1 - e^{-j\omega_m}\right|^2 \tilde{u}_l(\boldsymbol{\omega})\right)_{l=1,\ldots,d} \in \mathbb{C}^d.$$

These approximations, along with the fact that $\cos\omega = (e^{j\omega} + e^{-j\omega})/2$ and $\sin\omega = (e^{j\omega} - e^{-j\omega})/2j$, are used in Sect. 3.1 in order to deduce equations (19), (25) and (29).

References

1. Abel, J.: Medical image processing info 2004–2007. www.medical-image-processing.info
2. Amit, Y.: A nonlinear variational problem for image matching. SIAM J. Sci. Comput. **15**(1), 207–224 (1994)
3. Bajcsy, R., Kovacic, S.: Multiresolution elastic matching. Comput. Vis. Graph. Image Process. **46**(1), 1–21 (1989)
4. Ben-Israel, A., Greville, T.N.E.: Generalized Inverses: Theory and Applications. Wiley, New York (1977)
5. Braumann, U.-D., Kuska, J.-P.: Influence of the boundary conditions on the results of non-linear image registration. IEEE Int. Conf. Image Process. **I**, 1129–1132 (2005)
6. Bro-Nielsen, M., Gramkow, C.: Fast fluid registration of medical images. In: Lecture Notes in Computer Science, vol. 1131, pp. 267–276. Springer, Berlin (1996)
7. Broit, C.: Optimal registration of deformed images. Ph.D. thesis, University of Pennsylvania (1981)
8. Brown, L.G.: A survey of image registration techniques. ACM Comput. Surv. **24**(4), 325–376 (1992)
9. Cachier, P., Bardinet, E., Dormont, D., Pennec, X., Ayache, N.: Iconic feature based nonrigid registration: the PASHA algorithm. Comput. Vis. Image Underst. **89**, 272–298 (2003)
10. Christensen, G.E.: Deformable shape models for anatomy. Ph.D. thesis, Washington University (1994)
11. Clarenz, U., Droske, M., Henn, S., Rumpf, M., Witsch, K.: Computational methods for nonlinear image registration. Math. Method Regist. Appl. Med. Imaging Math. Ind. **10**, 1–22 (2006)
12. D'Agostino, E., Maes, F., Vandermeulen, D., Suetens, P.: A viscous fluid model for multimodal non-rigid image registration using mutual information. Med. Image Anal. **7**, 565–575 (2003)
13. D'Agostino, E., Maes, F., Vandermeulen, D., Suetens, P.: Validation of non-rigid image registration using mutual information. Technical Report, Katholieke Universiteit Leuven, March 2004
14. Davis, P.J.: Circulant Matrices. Wiley-Interscience, New York (1979)
15. Fischer, B., Modersitzki, J.: Fast inversion of matrices arising in image processing. Numer. Algorithms **22**, 1–11 (1999)
16. Fischer, B., Modersitzki, J.: Fast diffusion registration. In: Nashed, M.Z., Scherzer, O. (eds.) Inverse Problems, Image Analysis, and Medical Imaging. Contemporary Mathematics, vol. 313, pp. 117–129. AMS (2002)
17. Fischer, B., Modersitzki, J.: Curvature based image registration. J. Math. Imaging Vis. **18**(1), 81–85 (2003)
18. Fischer, B., Modersitzki, J.: Fast image registration—a variational approach. In: Psihoyios, G. (ed.) Proceedings of the International Conference on Numerical Analysis & Computational Mathematics, pp. 69–74. Wiley, New York (2003)
19. Fischer, B., Modersitzki, J.: FLIRT: a flexible image registration toolbox. In: Lecture Notes in Computer Science, vol. 2717, pp. 261–270. Springer, Berlin (2003)
20. Fischer, B., Modersitzki, J.: A unified approach to fast image registration and a new curvature based registration technique. Linear Algebra Appl. **308**, 107–124 (2004)
21. Frigo, M., Johnson, S.G.: The design and implementation of FFTW3. Proc. IEEE **93**(2), 216–231 (2005)
22. Goshtasby, A.: Registration of images with geometric distortions. IEEE Trans. Geosci. Remote Sens. **26**, 60–64 (1988)
23. Haber, E., Modersitzki, J.: COFIR: coarse and fine image registration. In: SIAM Real-Time PDE-Constrained Optimization, pp. 37–49 (2007)
24. Hajnal, J., Hill, D., Hawkes, D.: Medical Image Registration. CRC Press, Boca Raton (2001)
25. Hata, N., Dohi, T., Warfield, S., Wells, W., Kikinis, R., Jolesz, F.A.: Multimodality deformable registration of pre- and intraoperative images for MRI-guided brain surgery. In: Lecture Notes in Computer Science, vol. 1496, pp. 1067–1074. Springer, Berlin (1998)
26. Henn, S.: A multigrid method for a fourth-order diffusion equation with application to image processing. SIAM J. Sci. Comput. **27**(3), 831–849 (2005)
27. Henn, S.: A full curvature based algorithm for image registration. J. Math. Imaging Vis. **24**(2), 195–208 (2006)
28. Henn, S.: A translation and rotation invariant Gauss-Newton like scheme for image registration. BIT Numer. Math. **46**, 325–344 (2006)
29. Henn, S., Witsch, K.: Multi-modal image registration using a variational approach. SIAM J. Sci. Comput. **23**(4), 1429–1447 (2004)
30. Henn, S., Witsch, K.: Image registration based on multiscale energy information. Multiscale Model. Simul. **4**(2), 584–609 (2005)
31. Hermosillo, G., Chefd'Hotel, C., Faugeras, O.: A variational approach to multi-modal image matching. Technical Report 4117, INRIA, February 2001
32. Lester, H., Arridge, S.: A survey of hierarchical non-linear medical image registration. Pattern Recognit. **32**, 129–149 (1999)
33. Maes, F., Vandermeulen, D., Suetens, P.: Medical image registration using mutual information. Proc. IEEE **91**, 1699–1722 (2003)
34. Maintz, J., Viergever, M.: A survey of medical image registration. Med. Image Anal. **2**(1), 1–36 (1998)
35. Miller, M.I., Christensen, G.E., Amit, Y., Grenader, U.: Mathematical textbook of deformable neuroanatomies. Proc. Natl. Acad. Sci. USA **24**, 11944–11948 (1993)
36. Modersitzki, J.: Numerical Methods for Image Registration. Oxford University Press, London (2004)
37. Oppenheim, A.V., Schafer, R.: Discrete-Time Signal Processing, 2nd edn. Prentice-Hall, Upper Saddle River (1999)
38. Papenberg, N., Schumacher, H., Heldmann, S., Wirtz, S., Bommersheim, S., Ens, K., Modersitzki, J., Fischer, B.: A fast and flexible image registration toolbox: design and implementation of the general approach. In: Bildverarbeitung fur die Medizin, pp. 106–110 (2007)
39. Research Center Caesar: Julius software development framework (1999–2006). www.julius.caesar.de
40. Roche, A., Malandain, G., Pennec, X., Ayache, N.: The correlation ratio as a new similarity measure for multimodal image registration. In: Lecture Notes in Computer Science, vol. 1496, pp. 1115–1124. Springer, Berlin (1998)

41. Rohr, K.: Landmark-based image analysis: using geometric and intensity models. In: Computational Imaging and Vision Series, p. 21. Kluwer Academic, Dordrecht (2001)
42. Thirion, J.-P.: Image matching as a diffusion process: an analogy with Maxwell's demons. Med. Image Anal. **2**(3), 243–260 (1998)
43. Tikhonov, A.N., Arsenin, V.Y.: Solutions of Ill-posed Problems. Winston and Sons, Washington (1977)
44. Wang, Y., Staib, L.H.: Elastic model based non-rigid registration incorporating statistical shape information. In: Lecture Notes in Computer Science, vol. 1496, pp. 1162–1173. Springer, Berlin (1998)
45. Zhang, Z., Jiang, Y., Tsui, H.: Consistent multi-modal non-rigid registration based on a variational approach. Pattern Recognit. Lett. **27**, 715–725 (2006)
46. Zitová, B., Flusser, J.: Image registration methods: a survey. Image Vis. Comput. **21**, 997–1000 (2003)

Jorge Larrey-Ruiz received the M.S. degree in Telecommunications Engineering in 2000 from the Technical University of Valencia, Spain, and the Ph.D. in the same field in 2008 from the Technical University of Cartagena, Spain, where he is currently a researcher and Assistant Professor of Signal and Communications Theory. His technical interests include image registration and fusion, and digital filtering.

Rafael Verdú-Monedero received the M.S. degree in Telecommunications Engineering in 2000 from the Technical University of Valencia, Spain, and the Ph.D. in the same field in 2005 from the Technical University of Cartagena, Spain. He is currently Assistant Professor of Signal and Communications Theory at Technical University of Cartagena. His technical interests are modelling and inverse problems in image analysis.

Juan Morales-Sánchez received the B.S. degree in 1992 from the University of Alcalá, Spain, the M.S. degree in Telecommunications Engineering in 1996 from the Technical University of Valencia, Spain, and the Ph.D. in the same field in 2005 from the Technical University of Cartagena, Spain. Since 1999, he has been involved in different research and development projects at Technical University of Cartagena, where he is currently Assistant Professor of Signal and Communications Theory. His technical interests include image processing and medical imaging.